

Phonon softening in paramagnetic bcc Fe and relationship with pressure-induced phase transition

Yuji Ikeda,^{1,*} Atsuto Seko,^{1,2} Atsushi Togo,¹ and Isao Tanaka^{1,2,3,†}

¹Center for Elements Strategy Initiative for Structure Materials (ESISM), Kyoto University, Kyoto 606-8501, Japan

²Department of Materials Science and Engineering, Kyoto University, Kyoto 606-8501, Japan

³Nanostructures Research Laboratory, Japan Fine Ceramics Center, Nagoya 456-8587, Japan

(Dated: September 27, 2018)

Structural stability of paramagnetic (PM) body-centered cubic (bcc) Fe under pressure is investigated based on first-principles phonon calculations. Spin configurations of the PM phase are approximated using a binary special quasi-random structure (SQS) with a supercell approach. The behavior of phonon modes can be associated with pressure-induced phase transitions to the face-centered cubic (fcc) and hexagonal close-packed (hcp) structures as follows: For the PM phase, it is found that the low-frequency transverse mode at the N point (N_4^- mode), which corresponds to a bcc-hcp phase transition pathway, exhibits strong softening under isotropic volume compression. The frequency of this mode becomes zero by 2% volume decrease within the harmonic approximation. This result is not consistent with the experimental fact that phase transition from the PM bcc to hcp phases does not occur under volume compression. The seeming contradiction can be explained only when anharmonic behavior of the N_4^- mode is taken into consideration; a potential energy curve along the N_4^- mode becomes closer to a double-well shape for the PM phase under the volume compression. On the other hand, softening of the longitudinal mode at the $2/3[111]$ point under the volume compression is also found for the PM phase, which indicates the pressure-induced bcc-fcc phase transition along this mode. Such behaviors are not seen in ferromagnetic (FM) bcc Fe, implying that the magnetic structure plays essential roles on the phase transition mechanism.

PACS numbers: 71.15.Mb, 75.50.Bb, 63.20.dk

I. INTRODUCTION

The elemental Fe is widely known to exhibit several structural and magnetic phases, which have been investigated over many years. Figure 1 shows an experimental phase diagram for the elemental Fe.¹⁻⁴ Three stable phases, namely body-centered cubic (bcc), face-centered cubic (fcc), and hexagonal close-packed (hcp) exist as solid phases. They can be further classified by magnetic structures, i.e., ferromagnetic (FM) and paramagnetic (PM) phases. At ambient pressure, the stable phase changes as FM bcc \rightarrow PM bcc \rightarrow PM fcc \rightarrow PM bcc with increase of temperature. At room temperature, the elemental Fe undergoes a pressure-induced bcc-hcp phase transition at 9.2 GPa. Above the temperature of the triple point where the three phases coexist at 678 K and 8.2 GPa, bcc-fcc phase transition occurs.

Analysis of structural stability is an important approach to investigate the phase transition behavior. From the theoretical viewpoint, the structural stability of crystalline materials can be analyzed using a combination of density functional theory (DFT) and phonon calculations. Therefore, an additional method is required to analyze the structural stability of high temperature phases. The PM phase of Fe is a typical example. In recent years, several calculation methods for obtaining phonon frequencies of the PM phase have been proposed. Leonov *et al.* reported a method based on the dynamical mean-field theory (DMFT).⁵ They succeeded to reproduce experimental phonon dispersion relations for both PM bcc and PM fcc Fe.^{6,7} Körmann *et al.* developed a method for

calculating phonon frequencies for the PM phase⁸ based on the binary special quasi-random structure (SQS).⁹ In this method, force constants for the PM phase were obtained by a symmetrization process. Their results for the PM bcc and PM fcc Fe were also consistent with the experimental ones.^{6,7} Ruban and Razumovskiy proposed another way to approximate the PM phase using several spin spiral states.¹⁰

The present study aims at elucidating the behavior of phonons in the PM phase under pressure by means of systematic DFT-based phonon calculations. We adopt a method equivalent to that reported in Ref. 8 to obtain phonon frequencies of the PM phase. Volume dependence of the phonon frequencies and the potential energy curves along phonon modes are investigated in order to examine their anharmonic behaviors. Results are mainly discussed from the viewpoint of the pressure-induced phase transition for the PM bcc Fe.

II. METHODOLOGY

A. Modeling of PM phase

In principle, a magnetic state at finite temperature is described as the statistical average of all possible spin configurations. For the PM phase, instead of evaluating the statistical average, a completely disordered spin configuration is often used for simplicity. The SQS mimics such a disordered configuration within a periodic structure.⁹ The SQS originates from the cluster ex-

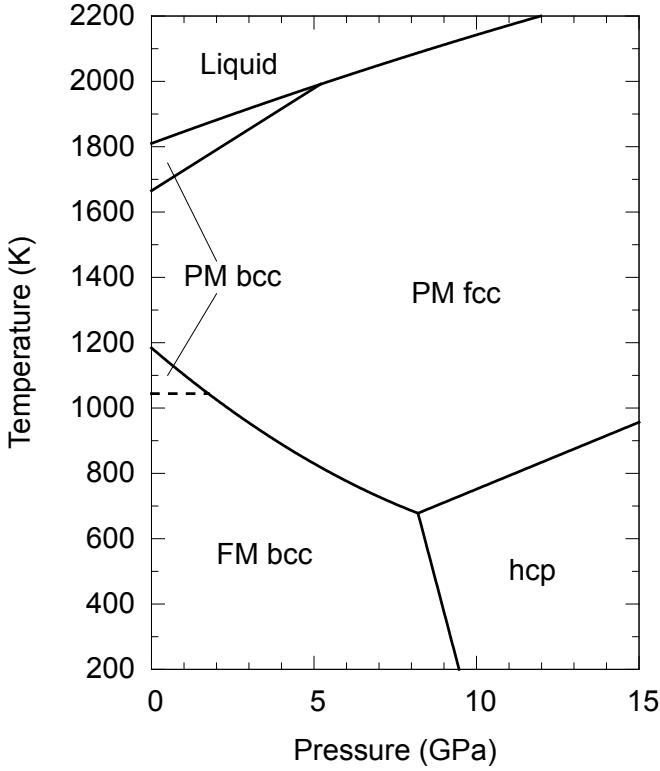


FIG. 1. Experimental phase diagram of Fe.¹⁻⁴ Solid and dashed bold lines represent structural and magnetic phase boundaries, respectively. For the magnetic structure of the hcp phase, both nonmagnetic (NM) and anti-ferromagnetic phases have been proposed.

pansion method which corresponds to generalized Ising model. Here the binary SQS is applied to the completely disordered collinear spin configuration. The SQS is generated from a supercell obtained by $2 \times 2 \times 2$ isotropic expansion of the conventional bcc unit cell. The isotropic expansion is adopted here because force constants of the PM phase are easily computed. The SQS generated from the $2 \times 2 \times 2$ supercell was reported to be sufficient to reproduce the experimental phonon dispersion relations of the PM bcc Fe.⁸ With the constraint of the supercell, pair correlation functions up to several nearest neighbors are optimized using simulated annealing procedure as implemented in the CLUPAN code.^{11,12}

B. Phonon calculations

Phonon frequencies are calculated by means of the finite-difference method with a displacement of 0.01 \AA . For the FM and NM phases, atomic displacements are given to the $2 \times 2 \times 2$ supercell of a conventional bcc unit cell, and the forces acting on atoms are collected. Force constants are calculated from the set of forces in the least-squares sense.^{13,14}

Before the depiction of how to obtain the force con-

stants of the PM phase, we briefly describe calculation procedure of the force constants for the FM and NM phases. We use R and τ for the index of unit cells and the index of atoms in the corresponding unit cell, respectively. A second-order force constant is denoted as $\Phi_{R_i\tau_i, R_j\tau_j}^{\alpha\beta}$, where the superscripts α and β are used for the indices of Cartesian coordinates, and the subscripts $R_i\tau_i$ and $R_j\tau_j$ specify a pair of atoms. For computational convenience, the force constants for a pair of atoms, $R_1\tau_1$ and $R_2\tau_2$, are represented by a 9×1 matrix $\mathbf{P}(R_1\tau_1, R_2\tau_2)$ given by

$$\mathbf{P}(R_1\tau_1, R_2\tau_2) = \begin{pmatrix} \Phi_{R_1\tau_1, R_2\tau_2}^{xx} \\ \Phi_{R_1\tau_1, R_2\tau_2}^{xy} \\ \Phi_{R_1\tau_1, R_2\tau_2}^{xz} \\ \Phi_{R_1\tau_1, R_2\tau_2}^{yx} \\ \Phi_{R_1\tau_1, R_2\tau_2}^{yy} \\ \Phi_{R_1\tau_1, R_2\tau_2}^{yz} \\ \Phi_{R_1\tau_1, R_2\tau_2}^{zx} \\ \Phi_{R_1\tau_1, R_2\tau_2}^{zy} \\ \Phi_{R_1\tau_1, R_2\tau_2}^{zz} \end{pmatrix}. \quad (1)$$

In addition, an atomic displacement applied to the atom $R_1\tau_1$ is described as a 3×9 matrix $\mathbf{U}_i(R_1\tau_1)$ given by

$$\mathbf{U}_i(R_1\tau_1) = \begin{pmatrix} 1 & 0 & 0 \\ 0 & 1 & 0 \\ 0 & 0 & 1 \end{pmatrix} \otimes (\Delta x \ \Delta y \ \Delta z), \quad (2)$$

where Δx , Δy , and Δz represent Cartesian components of the displacement given to the atom $R_1\tau_1$, and the subscript i is for the index of atomic displacements. For the system with the displacement $\mathbf{U}_i(R_1\tau_1)$, a force acting on the atom $R_2\tau_2$ can be written in the form of a 3×1 matrix $\mathbf{F}_i(R_2\tau_2)$ as

$$\mathbf{F}_i(R_2\tau_2) = \begin{pmatrix} F_x \\ F_y \\ F_z \end{pmatrix}, \quad (3)$$

where F_x , F_y , and F_z are Cartesian components of the force acting on the atom $R_2\tau_2$. We can obtain $\mathbf{F}_i(R_2\tau_2)$ using $\mathbf{P}(R_1\tau_1, R_2\tau_2)$ and $\mathbf{U}_i(R_1\tau_1)$ as

$$\mathbf{F}_i(R_2\tau_2) = -\mathbf{U}_i(R_1\tau_1)\mathbf{P}(R_1\tau_1, R_2\tau_2). \quad (4)$$

Simultaneous equations of different atomic displacements for the pair of atoms are then combined as

$$\begin{pmatrix} \mathbf{F}_1 \\ \mathbf{F}_2 \\ \vdots \end{pmatrix} = - \begin{pmatrix} \mathbf{U}_1 \\ \mathbf{U}_2 \\ \vdots \end{pmatrix} \mathbf{P}. \quad (5)$$

With a sufficient number of atomic displacements, Eq. (5) can be solved by the pseudoinverse such as

$$\mathbf{P} = - \begin{pmatrix} \mathbf{U}_1 \\ \mathbf{U}_2 \\ \vdots \end{pmatrix}^+ \begin{pmatrix} \mathbf{F}_1 \\ \mathbf{F}_2 \\ \vdots \end{pmatrix}. \quad (6)$$

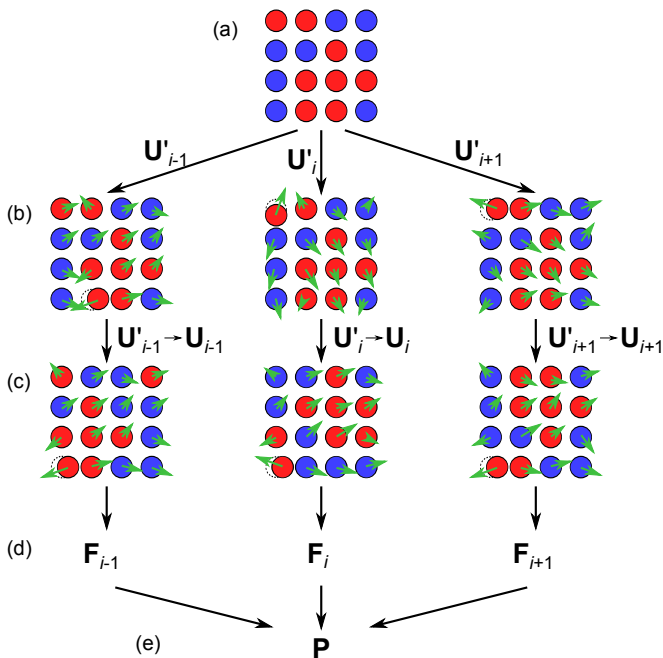


FIG. 2. (Color online) Two dimensional schematic illustration of the procedure to obtain the force constants of the PM phase. Red and blue circles represent atoms with spin-up and spin-down magnetic moments, respectively. Green small arrows on the circles represent the forces acting on the atoms. (a) The completely disordered spin configuration is mimicked by the binary SQS. (b) Symmetrically inequivalent displacements U'_i are applied to the SQS. (c) The displaced atoms are moved to one of the crystallographically equivalent sites of the supercell without magnetic moments. By this operation, U'_i is changed to U_i . (d) The forces acting on the atoms F_i are calculated. (e) From all the configurations with the displacements, the forces are collected, and the force constants of the PM phase are obtained via Eq. (6).

To recover site symmetry around the displaced atom, we apply the site-symmetry operations to the atomic system and obtain new displacements and corresponding forces. By adding these displacements and forces to the simultaneous equations shown in Eq. (5), we can obtain symmetry-recovered force constants. Note that for the atoms at the crystallographically equivalent sites, we need to apply displacements only to one of them; by considering the symmetry of the structure, force constants for the other atoms can be derived without calculations via Eq. (6).

To calculate the force constants of the PM phase, a symmetrization procedure is applied as follows: First, we consider the binary SQS to mimic a completely disordered spin configurations (Fig. 2(a)). For the SQS, symmetrically inequivalent displacements $U'_i(R_1\tau_1')$ are applied (Fig. 2(b)). Next, for the system with $U'_i(R_1\tau_1')$, we apply a symmetry operation which moves the displaced atom $R_1\tau_1'$ to $R_1\tau_1$, where $R_1\tau_1$ is the atom on the crystallographically equivalent site to that for the

atom $R_1\tau_1$, when we neglect the local magnetic moments. By this operation, the displacement $U'_i(R_1\tau_1')$ is changed to $U_i(R_1\tau_1)$ (Fig. 2(c)). For the system with $U_i(R_1\tau_1)$, a force acting on the atom $R_2\tau_2$, $F_i(R_2\tau_2)$, is obtained (Fig. 2(d)). From all systems, the displacements $U_i(R_1\tau_1)$ and the forces $F_i(R_2\tau_2)$ are collected, and the force constants $P(R_1\tau_1, R_2\tau_2)$ are calculated via Eq. (6) as well as the FM and NM cases (Fig. 2(e)).

In this study, we assume that many completely disordered spin configurations appear in a shorter time than that for the thermal atomic fluctuations in the PM phase. The present averaging process includes effects from many disordered spin configurations, and hence we can represent the PM phase by this process. By considering the site symmetry around the displaced atom, the symmetry of the original structure can be recovered by the same procedure as the FM and NM cases.

The force constants obtained by this procedure are regarded as those of the PM phase. For example, if we use the SQS constructed from the $2 \times 2 \times 2$ supercell of the conventional bcc unit cell, the obtained force constants can be regarded as those for the $2 \times 2 \times 2$ supercell in the PM phase. These PM force constants have the same symmetry as those of the supercell without magnetic moments. This approach can be applied not only to the disordered magnetic states but also to chemically disordered compounds. Actually, the present procedure is equivalent to that introduced in Ref. 8. The only difference is that in the present case, we first collect forces on the atoms, while for the procedure in Ref. 8, they first made the force constants from each spin configuration and then took average of the set of the force constants. We found that both the procedures provide almost the same result for the PM bcc Fe.

The calculations of phonon frequencies are performed by the PHONOPY code.¹⁵

C. Conditions for electronic structure calculations

For the first-principles electronic structure calculations, the plane-wave basis projector augmented wave (PAW) method¹⁶ is employed in the framework of DFT within the generalized gradient approximation in the Perdew-Burke-Ernzerhof form¹⁷ as implemented in the VASP code.¹⁸⁻²⁰ A plane-wave energy cutoff of 300 eV is used. The radial cutoff of the PAW potential of Fe is 1.22 Å. The 3d and 4s electrons for Fe are treated as valence and the remaining electrons are kept frozen. The Brillouin zones are sampled by a Γ -centered $16 \times 16 \times 16$ k -point mesh per conventional bcc unit cell, and the Methfessel-Paxton scheme²¹ with a smearing width of 0.1 eV is employed. The total energy is minimized until the energy convergence becomes less than 1×10^{-8} eV. For the calculations of the PM phase, the difference between the numbers of spin-up and spin-down electrons is fixed to be zero.

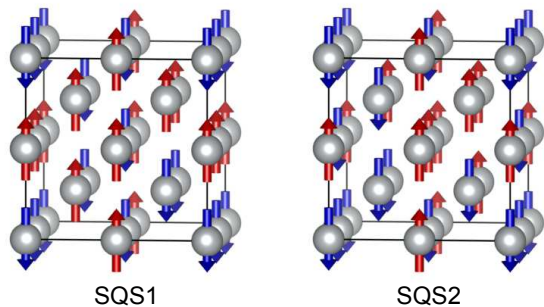


FIG. 3. (Color online) Two kinds of binary SQSs for the bcc structure investigated in this study. These SQSs are constructed from a supercell obtained by $2 \times 2 \times 2$ isotropic expansion of the conventional bcc unit cell and hence include 16 atoms. The completely disordered collinear spin configuration is mimicked by these SQSs. Up (red) and down (blue) arrows represent atoms with spin-up and spin-down magnetic moments, respectively. Visualization is performed using the VESTA code.²²

TABLE I. Pair correlation functions for the SQSs shown in Fig. 3. For SQS1 and SQS2, the pair correlation functions up to the fifth and the fourth nearest neighbor are optimized by the least absolute deviation method, respectively.

Pair correlation function	SQS1	SQS2
1st NN	0	0
2nd NN	0	0
3rd NN	$-1/3$	0
4th NN	0	0
5th NN	0	-1

III. RESULTS AND DISCUSSION

A. Dependence on the selection of SQS

First, we investigate the dependence of the results for the PM phase on the pair correlation functions of the

TABLE II. Calculated equilibrium volume at the pressure of 0 GPa and the temperature of 0 K for the FM, PM, and NM bcc Fe. Energy differences between the magnetic phases are also described. The energy of the FM phase is set to the origin for the energy differences. For the PM phase, values derived from the two kinds of SQSs are shown, and the SQSs for the values are given in the parentheses in the first column. Note that zero point vibrational contributions are not included.

Magnetic phase	Volume ($\text{\AA}^3/\text{atom}$)	ΔE (eV/atom)
FM	11.3	0.00
PM(SQS1)	11.3	0.20
PM(SQS2)	11.4	0.19
NM	10.5	0.47

SQS. For this purpose, two kinds of binary SQSs which have different correlation functions are considered. These two SQSs, i.e., SQS1 and SQS2, are described in Fig. 3. Table I shows the values of their pair correlation functions. The pair correlation functions up to the fifth and the fourth nearest neighbor are optimized for SQS1 and SQS2 by the least absolute deviation method, respectively. Table II shows the calculated equilibrium volume at the pressure of 0 GPa and the temperature of 0 K, V_0 , for the FM, PM, and NM bcc Fe. For the PM phase, we find that the two SQSs provide almost the same volumes and energies. This indicates that the results of the PM phase do not depend on the details of the correlation functions of the SQSs. In other words, if the values of several principal pair correlation functions are chosen to be equal to those of the completely disordered spin configuration, the difference of the results is negligible. Therefore, we will hereafter show only the results from the SQS1 for the PM phase.

B. Phonon dispersion relations

Figure 4 shows calculated phonon dispersion relations at four values of volumes around the equilibrium one for each magnetic phase, V_0 (shown in Table II). It is found that the phonon frequencies of the PM phase tend to be smaller than those of the FM phase almost in the whole region. It is also confirmed that the lowest-frequency modes at the N and $2/3[111]$ points of the PM phase decrease their frequencies with decrease of volume. For the FM phase, such softenings under volume compression cannot be observed. This indicates that the two phonon modes characterize the structural stability of the PM bcc Fe. Hence we will hereafter discuss the behavior of the two phonons under volume compression in more detail.

At the N point, one of the transverse modes at the N point becomes softer under volume compression. (This mode has the irreducible representation of N_4^- , and hence we will hereafter refer to this mode as the N_4^- mode.) This mode finally becomes imaginary under a large volume compression. This means that the PM bcc Fe dynamically unstable under certain pressures within the harmonic approximation. From the calculations with 1% intervals of volume compression, we find that this imaginary mode appears from 2% volume compression.

Atomic displacements along the N_4^- mode can be associated with the well-known Burgers pathway.²³ This pathway is composed on two types of transformations: the displacement of adjacent (110) planes in opposite $[\bar{1}\bar{1}0]$ directions and the shear deformation along the $[001]$ direction. The former part corresponds to the N_4^- mode. The softening of the N_4^- mode is experimentally observed for several NM metals such as Ti, Zr, and Hf,^{24–26} and these metals actually show bcc-hcp phase transitions. Therefore, the softening of the N_4^- mode has been considered as a precursor of the phase transitions.

Experimentally, the PM bcc Fe undergoes pressure-

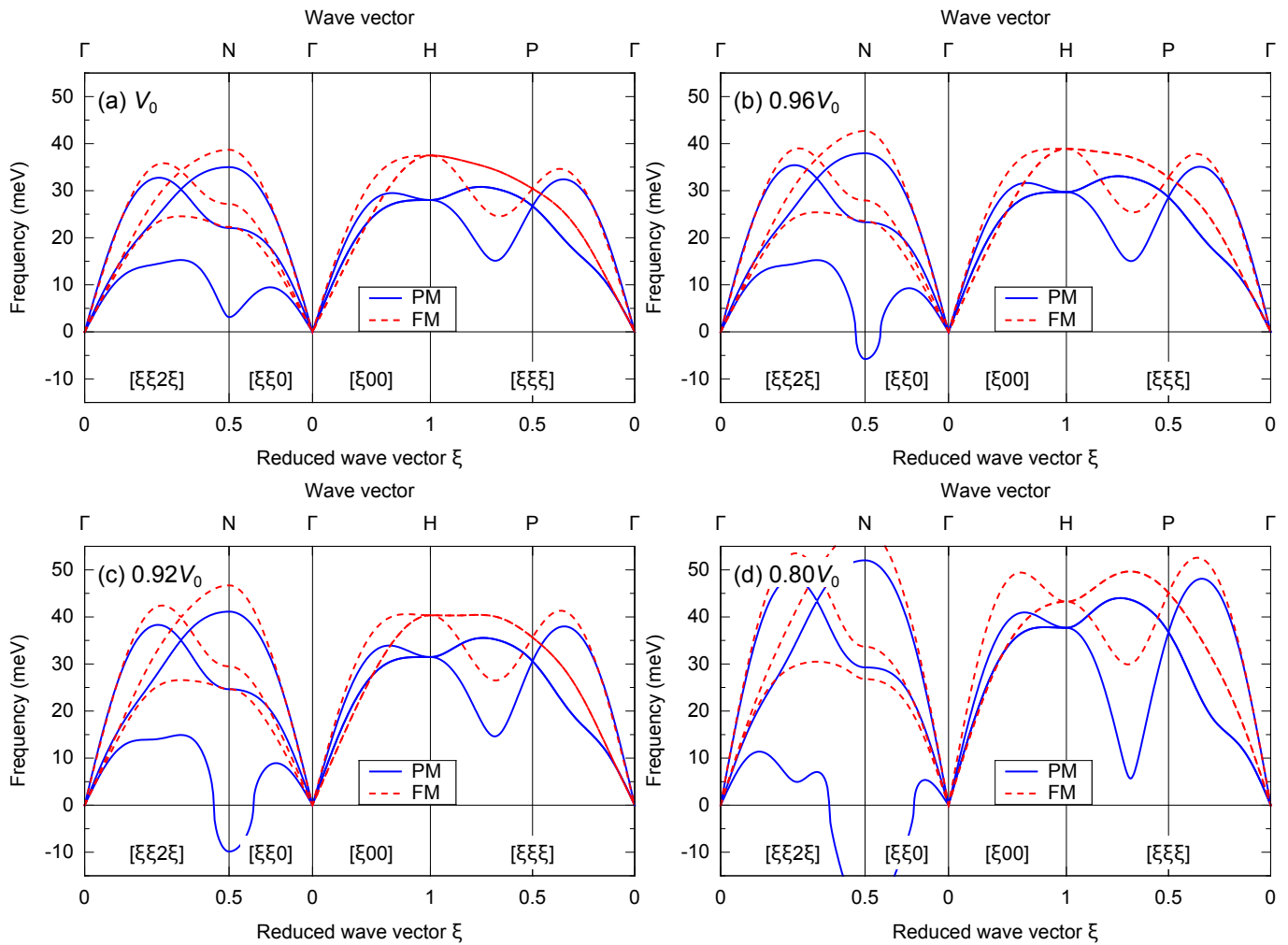


FIG. 4. (Color online) Calculated phonon dispersion relations at the volume of (a) V_0 , (b) $0.96V_0$, (c) $0.92V_0$, and (d) $0.80V_0$ for the bcc Fe, where V_0 is the equilibrium volume of each magnetic phase shown in Table II. Blue solid and red dashed curves are for the PM and FM phases, respectively. Note that a negative value of a phonon frequency corresponds to an imaginary mode.

induced phase transition to the fcc phase rather than the hcp one. However, the computational results for the N_4^- mode in the PM phase clearly becomes imaginary under volume compression, which seemingly indicates the spontaneous bcc-hcp phase transition along the Burgers pathway. This seeming contradiction can be ascribed to the neglect of anharmonic effects of the phonons at high temperature. To analyze anharmonic effects of the N_4^- phonon mode in more detail, potential energy curves along this mode are calculated around the equilibrium volume, $V_0 = 11.3\text{\AA}^3/\text{atom}$. The result is shown in Fig. 5. The energy of the PM phase with the displacements of the atoms is determined as follows: First we consider the configurations which are derived from the SQS by applying symmetry operations of the supercell corresponding to the SQS. Then we give the atomic displacements along the N_4^- mode to these configurations. Finally we take an average of the energies

obtained from them, which is regarded as the energy of the PM phase. Note that for the PM phase, several calculations with large atomic displacements encountered convergence problems. Therefore, results for several points in this region are not shown for the PM phase. It is clearly confirmed that the dependence of the energies on the phonon amplitude is much weaker for the PM phase than that for the FM phase. This causes atomic large thermal fluctuations of the atoms for the PM phase. We can also find that for the PM phase, the curve gets close to a double-well shape with decrease of volume. This means that the anharmonicity along the N_4^- mode becomes stronger as the volume decreases. This anharmonicity indicates that time-averaged atomic positions become the ideal ones for the bcc structure due to the large thermal fluctuations at sufficiently high temperature. Therefore, the bcc structure is stabilized along the N_4^- mode at the temperature and does not causes the

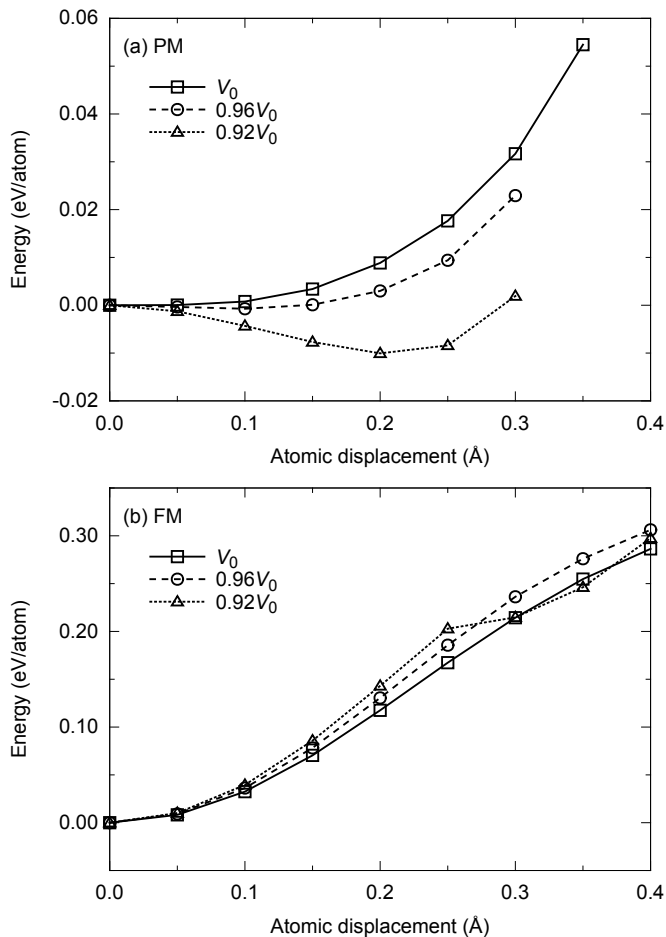


FIG. 5. Potential energy curves along the N_4^- mode with respect to volumes for the (a) PM and (b) FM phases. Square, circle, and triangle symbols are for the results at V_0 , $0.96V_0$, and $0.92V_0$, respectively, where V_0 denotes the equilibrium volume. Lines connecting the symbols are guides for the eyes.

spontaneous transition to the hcp phase. This idea is well consistent with experimental results.

To evaluate the anharmonicity of these curves more quantitatively, the curves are fitted by the fourth-order polynomial functions, $E(x) = E_0 + a_2x^2/2 + a_4x^4/4!$, where x , $E(x)$, E_0 , a_2 , and a_4 are the displacements of atoms, the energy at the corresponding displacements, the energy at the ideal bcc positions, the coefficient for the second order, and the coefficient for the fourth order, respectively. The fitting parameters, a_2 and a_4 , are determined by means of the least-squares method. The result is shown in Table III. The ratio between the second- and the fourth-order coefficients, a_4/a_2 , are also shown in this table. This ratio clarifies the fourth-order effect with respect to the second-order harmonic effect and can be considered as one of the indices to evaluate the strength of the anharmonicity. It is shown that the absolute values of the ratios for the PM phase are much larger than

that for the FM phase. This reveals strong anharmonicity of the N_4^- mode for the PM phase. We can also find that a_4 of the PM phase is positive at all of the three volumes, which makes the potential energy curve close to the double-well shape.

Recently, Mankovsky *et al.* have reported²⁷ the potential energy curves along the N_4^- mode of the PM bcc Fe based on the coherent potential approximation (CPA) in combination with the disordered local moment (DLM) scheme. Their result at the volume of $10.4\text{\AA}^3/\text{atom}$ ($\approx 0.92V_0$) showed that the energy of the PM bcc Fe along the N_4^- mode decreased monotonically (see Fig. 4(c) in Ref. 27). This result is different from that from the present SQS-based approach which shows the double-well potential. The major source of the inconsistency may be caused by the anharmonic effects of the phonons rather than the difference of the theoretical treatment for the PM phases.

In Fig. 4, we can also find the softening of the longitudinal phonon mode at the $2/3[111]$ point under volume compression. This mode consists in the displacement of the (111) planes along the [111] direction, which corresponds to a bcc- ω phase transition pathway. Similar to the case of the phonon mode at the N point, the softening has been experimentally observed for the NM metals such as Ti, Zr, and Hf, which actually show the bcc- ω phase transitions.²⁴⁻²⁶ Recently, our group proposed²⁸ a novel bcc-fcc phase transition pathway where the ω structure appears as an energy barrier during the bcc-fcc transformation. The present finding implies that the softening of the longitudinal mode at the $2/3[111]$ point can be considered as a precursor for the bcc-fcc transition as well as that for the bcc- ω transition. Actually, this is consistent with the experimental fact that the PM bcc Fe undergoes the phase transition to the PM fcc Fe under pressure.

IV. SUMMARY

Structural stability of the PM bcc Fe under pressure is analyzed in detail based on the phonon dispersion relations. The PM phase is described using the binary SQS. In order to obtain the phonon frequencies for the PM phase, symmetrization procedure is applied. For the PM phase, the low-frequency transverse mode at the N point, which correspond to the bcc-hcp phase transition pathway, shows strong softening under volume compression. This mode becomes imaginary by 2% volume decrease within the harmonic approximation. This result seems contradictory to the experimental fact that phase transition from the PM bcc to hcp phases does not occur under compression. However, this puzzle can be solved by taking anharmonic behavior of the N_4^- into consideration; potential energy curves along the N_4^- mode for the PM phase is found to become a double-well shape under compression. We also find the softening at the longitudinal phonon mode at the $2/3[111]$ point under volume compression. This mode can be associated with the bcc-fcc

TABLE III. Fitting parameters to the calculated potential energy curves. The fourth-order polynomial functions $E(x) = E_0 + a_2x^2/2 + a_4x^4/4!$ is considered, where x , $E(x)$, E_0 , a_2 , and a_4 are the atomic displacement, the energy at the corresponding displacements, the energy at the ideal bcc positions, the coefficient for the second order, and the coefficient for the fourth order, respectively. The coefficients a_2 and a_4 are the fitting parameters and determined by means of the least-squares method.

Volume	Magnetic phase	a_2 (eV/(atom·Å ²))	a_4 (eV/(atom·Å ⁴))	a_4/a_2 (Å ⁻²)
V_0	PM	0.2	66.9	324.1
	FM	6.4	-217.3	-33.7
$0.96V_0$	PM	-0.2	89.2	-558.9
	FM	7.2	-257.7	-35.7
$0.92V_0$	PM	-0.9	131.9	-139.1
	FM	7.3	-287.0	-39.1

phase transition pathway where the ω structure appears during the transformation. Hence the softening of this mode can be considered as a precursor of the phase transition from PM bcc to PM fcc phases, which is indeed observed experimentally. Such softening behaviors are not observed for the FM phase, which implies that the phase transition mechanism is essentially different between the

FM and PM phases.

ACKNOWLEDGMENTS

The authors thank F. Körmann for valuable discussions. This work was supported by MEXT Japan through Elements Strategy Initiative for Structural Materials (ESISM) of Kyoto University.

* ikeda.yuji.6m@kyoto-u.ac.jp

† tanaka@cms.mtl.kyoto-u.ac.jp

¹ J. M. Leger, C. Loriers-Susse, and B. Vodar, Phys. Rev. B **6**, 4250 (1972).

² H. Strong, R. Tuft, and R. Hanneman, Metallurgical Transactions **4**, 2657 (1973).

³ G. Shen, H.-k. Mao, R. J. Hemley, T. S. Duffy, and M. L. Rivers, Geophysical Research Letters **25**, 373 (1998).

⁴ S. Klotz, Y. Le Godec, T. Strssle, and U. Stuhr, Applied Physics Letters **93**, 091904 (2008).

⁵ I. Leonov, A. I. Poteryaev, V. I. Anisimov, and D. Vollhardt, Phys. Rev. B **85**, 020401 (2012).

⁶ J. Zarestky and C. Stassis, Phys. Rev. B **35**, 4500 (1987).

⁷ J. Neuhaus, W. Petry, and A. Krimmel, Physica B **234-236**, 897 (1997).

⁸ F. Körmann, A. Dick, B. Grabowski, T. Hickel, and J. Neugebauer, Phys. Rev. B **85**, 125104 (2012).

⁹ A. Zunger, S.-H. Wei, L. G. Ferreira, and J. E. Bernard, Phys. Rev. Lett. **65**, 353 (1990).

¹⁰ A. V. Ruban and V. I. Razumovskiy, Phys. Rev. B **85**, 174407 (2012).

¹¹ A. Seko, K. Yuge, F. Oba, A. Kuwabara, I. Tanaka, and T. Yamamoto, Phys. Rev. B **73**, 094116 (2006).

¹² A. Seko, Y. Koyama, and I. Tanaka, Phys. Rev. B **80**, 165122 (2009).

¹³ K. Parlinski, Z. Q. Li, and Y. Kawazoe, Phys. Rev. Lett. **78**, 4063 (1997).

¹⁴ L. Chaput, A. Togo, I. Tanaka, and G. Hug, Phys. Rev. B **84**, 094302 (2011).

¹⁵ A. Togo, F. Oba, and I. Tanaka, Phys. Rev. B **78**, 134106 (2008).

¹⁶ P. E. Blöchl, Phys. Rev. B **50**, 17953 (1994).

¹⁷ J. P. Perdew, K. Burke, and M. Ernzerhof, Phys. Rev. Lett. **77**, 3865 (1996).

¹⁸ G. Kresse, J. Non-Cryst. Solids **192-193**, 222 (1995).

¹⁹ G. Kresse and J. Furthmüller, Comput. Mater. Sci. **6**, 15 (1996).

²⁰ G. Kresse and D. Joubert, Phys. Rev. B **59**, 1758 (1999).

²¹ M. Methfessel and A. T. Paxton, Phys. Rev. B **40**, 3616 (1989).

²² K. Momma and F. Izumi, J. Appl. Crystallogr. **44**, 1272 (2011).

²³ W. Burgers, Physica **1**, 561 (1934).

²⁴ W. Petry, A. Heiming, J. Trampenau, M. Alba, C. Herzig, H. R. Schober, and G. Vogl, Phys. Rev. B **43**, 10933 (1991).

²⁵ A. Heiming, W. Petry, J. Trampenau, M. Alba, C. Herzig, H. R. Schober, and G. Vogl, Phys. Rev. B **43**, 10948 (1991).

²⁶ J. Trampenau, A. Heiming, W. Petry, M. Alba, C. Herzig, W. Miekeley, and H. R. Schober, Phys. Rev. B **43**, 10963 (1991).

²⁷ S. Mankovsky, S. Polesya, H. Ebert, W. Bensch, O. Mathon, S. Pascarelli, and J. Minár, Phys. Rev. B **88**, 184108 (2013).

²⁸ A. Togo and I. Tanaka, Phys. Rev. B **87**, 184104 (2013).